Current Biology 20, 161–169, January 26, 2010 ©2010 Elsevier Ltd All rights reserved DOI 10.1016/j.cub.2009.11.036

Report

Movement Directionality in Collective Migration of Germ Layer Progenitors

Yohanna Arboleda-Estudillo,[1,2] Michael Krieg,[2] Jan Stühmer,[1] Nicholas A. Licata,[3] Daniel J. Muller,[2] and Carl-Philipp Heisenberg[1,*]

[1]Max Planck Institute of Molecular Cell Biology and Genetics, Pfotenhauerstrasse 108, D-01307 Dresden, Germany

[2]Biotechnology Center, Technische Universität Dresden, Tatzberg 47/49, D-01307 Dresden, Germany

[3]Max Planck Institute for the Physics of Complex Systems, Nöthnitzer Strasse 38, D-01187 Dresden, Germany

Summary

Collective cell migration, the simultaneous movement of multiple cells that are connected by cell-cell adhesion, is ubiquitous in development, tissue repair, and tumor metastasis [1, 2]. It has been hypothesized that the directionality of cell movement during collective migration emerges as a collective property [3, 4]. Here we determine how movement directionality is established in collective mesendoderm migration during zebrafish gastrulation. By interfering with two key features of collective migration, (1) having neighboring cells and (2) adhering to them, we show that individual mesendoderm cells are capable of normal directed migration when moving as single cells but require cell-cell adhesion to participate in coordinated and directed migration when moving as part of a group. We conclude that movement directionality is not a de novo collective property of mesendoderm cells but rather a property of single mesendoderm cells that requires cell-cell adhesion during collective migration.

Results and Discussion

Collective behavior has been observed in diverse biological systems, ranging from bird flocks and social insect colonies to the collective migration of cells in development and disease [3–5]. A hallmark of such systems is that the collective behavior of many individuals is not necessarily explained by the autonomous behavior of its individual components. Studies on collective cell migration in vitro and in vivo have shown that the biased motion of a small proportion of cells is in principle sufficient to direct the migration of a large body of cells [3, 4, 6]. It has therefore been suggested that movement directionality emerges as a collective property of cells moving together, although it is still unclear how broadly this applies to different forms of collective migration. To investigate how movement directionality could arise during collective migration in vivo, we analyzed the movement of germ layer progenitor cells during zebrafish gastrulation. Specifically, we focused on mesoderm and endoderm (mesendoderm) progenitors originating from lateral domains of the early gastrula known to display directed migration during midgastrulation stages (7–9 hours postfertilization [hpf]) [7]. To ascertain that these mesendoderm progenitors undergo collective migration, we analyzed their movement coordination and directionality, key features of collective migration [1, 2], in two-photon excitation microscopy movies detecting nuclei. Confirming and extending previous studies [7], we found that mesendoderm progenitors during midgastrulation stages (7–9 hpf) displayed highly coordinated and directed movements oriented toward the forming embryonic body axis as determined by their instantaneous speed (the speed at a particular moment), displacement speed, displacement effectiveness, and movement similarity [8] (Figures 1A–1F; see also Figure S1 available online), indicative for collective migration.

To investigate whether movement directionality is a collective property of mesendoderm cells moving together, we first asked how single mesendoderm cells migrate apart from their group. If movement directionality is a collective property, single mesendoderm progenitors are expected to exhibit poor directionality. We analyzed this by performing a series of cell transplantation experiments in which a single mesendoderm donor cell was placed into either the forming paraxial mesendoderm of a wild-type host embryo at the onset of gastrulation (6 hpf) or into an equivalent position in a maternal-zygotic *oep* (MZ*oep*) mutant embryo, which lacks most mesendoderm [9] (Figure 2A). Donor cell movements were recorded by confocal microscopy throughout mid and late gastrulation stages (7–10 hpf), allowing us to compare the migration of individual donor cells in the presence or absence of neighboring mesendoderm cells. We found that single donor mesendoderm progenitors in MZ*oep* mutants exhibited directed movements similar to those in wild-type embryos, as determined by their mean squared displacement instantaneous speed and effective speed (the speed of displacement; Figures 2B–2D). Moreover, single donor mesendoderm progenitors in MZ*oep* mutants moved in a preferred dorsal-vegetal direction toward the emerging body axis, indistinguishable from single donor progenitors in wild-type embryos (Figures 2E and 2F). This shows that individual mesendoderm progenitors in the absence of neighboring cells can undergo directed migration similar to mesendoderm progenitors undergoing collective migration. It further suggests that mesendoderm movement directionality is a property of individual mesendoderm progenitors rather than a collective property of these cells moving together in collective migration.

In addition to the ability of individual mesendoderm cells to undergo directed migration, external factors attributed to the presence of neighboring cells, particularly cell-cell adhesion, may influence directionality. To address whether cell-cell adhesion is involved in determining movement directionality during collective mesendoderm migration, we analyzed the movement of mesendoderm cells with impaired cell-cell adhesion. We modulated cell-cell adhesion by injecting discrete quantities of a *morpholino* antisense oligonucleotide (MO) to E-cadherin [10]. The amount of E-cadherin at the plasma membrane was found to scale with the amount of *e-cadherin* MO injected (Figure 3A), demonstrating a concentration-dependent effect of *e-cadherin* MO on E-cadherin expression in mesendoderm progenitors. To ascertain the effect on mesendoderm cell-cell adhesion, we correlated the amount of *e-cadherin* MO injected and E-cadherin at the plasma membrane with the cell-cell adhesion strength of

*Correspondence: heisenberg@mpi-cbg.de

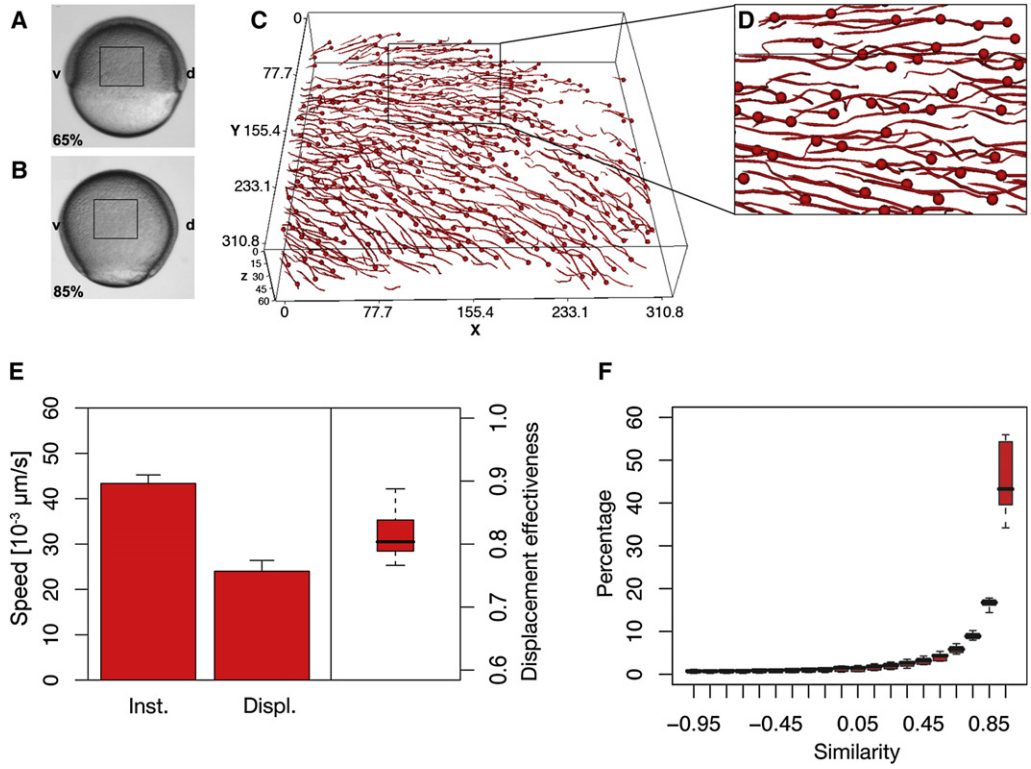

Figure 1. Movement of Lateral Mesendoderm Cells in Wild-Type Embryos

(A and B) Bright-field images of an embryo at the beginning of gastrulation (6.5 hours postfertilization [hpf]; A) and at midgastrulation (8.5 hpf; B). Boxes outline the imaged region in (C).

(C) Trajectories of mesendoderm progenitors during midgastrulation stages. Nuclei were tracked with nuclei tracking software [8]. The endpoint of each track is indicated with a sphere. The box depicts the magnified region shown in (D). Embryos were imaged by two-photon excitation microscopy from 6.5 hpf to 8.5 hpf. Animal pole is to the top and dorsal to the right.

(D) Magnified view of the boxed region in (C).

(E) Average instantaneous speed (inst.), average displacement speed (displ.), and displacement effectiveness of mesendoderm progenitors during midgastrulation stages.

(F) Instantaneous similarity of mesendoderm progenitor movements within a maximum distance of 20 μm. Values range from −1.0 (opposite direction of movement) over 0 (movement vectors are orthogonal) to +1 (parallel movement). Histograms were generated separately for each embryo. Box plots show the distribution of the bin heights among the different embryos.

mesendoderm progenitors as measured by single-cell force spectroscopy (SCFS) [10]. We found that the cell-cell adhesion force of both homotypic (morphant-to-morphant) and heterotypic (wild-type-to-morphant) cell-cell contacts scaled with the amount of *e-cadherin* MO injected (Figures 3A–3D) and the amount of E-cadherin at the plasma membrane (Figure 3E). When high levels of *e-cadherin* MO (8 ng per embryo) were injected, both E-cadherin expression and homotypic cell-cell adhesion were strongly reduced (Figures 3B–3D), in agreement with previous findings [10] that E-cadherin plays an important role in mesendoderm cell-cell adhesion. In contrast, cortex tension of individual mesendoderm progenitors as determined by colloidal force spectroscopy [10] remained unchanged in *e-cadherin* morphant cells (Figure 3F), suggesting that E-cadherin does not affect the cortical cytoskeleton.

To investigate how the demonstrated changes in cell-cell adhesion affect an individual mesendoderm progenitor's movement as part of a group, we used a cell transplantation assay, allowing us to simultaneously monitor the movements of mesendoderm progenitors with different adhesive strengths. Typically, a differentially labeled mix of control and experimental cells, ideally consisting of one cell each, was transplanted into the forming paraxial mesendoderm of a wild-type embryo at the onset of gastrulation (6 hpf), and the donor cell movements were recorded by confocal microscopy throughout mid and late gastrulation stages (7–10 hpf; Figures 4A–4C; Movie S1). We found that mesendoderm progenitors with lower cell-cell adhesion displayed significantly less directed movements, as revealed by their mean squared displacement and effective movement speed (Figures 4D and 4E). Moreover, mesendoderm progenitors with reduced cell adhesion failed to move in a preferred dorsal-vegetal direction toward the emerging body axis and instead showed dorsal-directed movements with little bias along the animal-vegetal axis (Figures 4F–4J). Plotting movement directionality as a function of cell-cell adhesion force, we found that the effective movement speed of mesendoderm progenitors linearly scaled with the adhesion force of both homotypic and heterotypic cell-cell contacts (Figure 4K). This shows that mesendoderm heterotypic cell-cell adhesion strength and effective movement speed are tightly correlated with each other ($r = 0.96$, $p = 0.009$), suggesting that adhesion-mediated mechanical coupling of cells is critical for directed movement of mesendoderm progenitors. In contrast, the instantaneous movement speed was hardly affected in mesendoderm progenitors with reduced cell-cell adhesion (Figure 4E; $r = 0.58$,

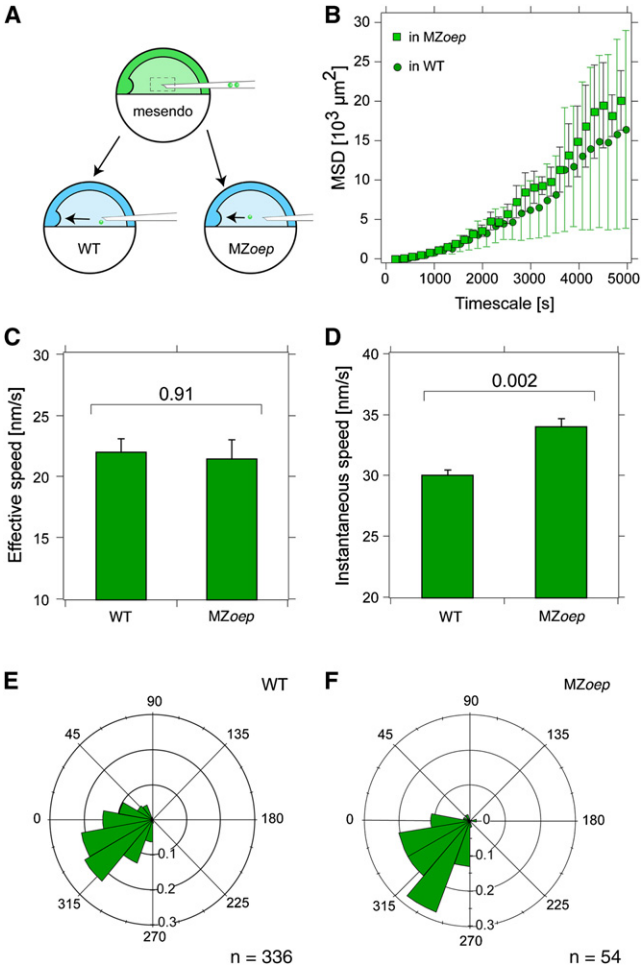

Figure 2. Movement of Individual Mesendoderm Cells in Wild-Type and MZ*oep* Mutant Embryos

(A) Schematic diagram of the cell transplantation experiment. One single mesendoderm cell was transplanted from a donor embryo into either wild-type (WT) or MZ*oep* mutant host embryos at the onset of gastrulation (6 hpf).

(B) Mean squared displacement (MSD) plot of individual mesendoderm donor cell movements in WT (circles) and MZ*oep* (squares) host embryos.

(C and D) Average effective (C) and instantaneous (D) speed of individual mesendoderm donor cell movements in WT and MZ*oep* host embryos.

(E and F) Movement orientation of individual mesendoderm donor cells in WT (E) and MZ*oep* (F) host embryos. n represents number of analyzed cells.

p = 0.31). This suggests that cell-cell adhesion predominantly affects the directionality rather than the general motility of individual mesendoderm movements in collective migration.

In our transplantation experiments described above, we analyzed how changes in donor cell adhesion interfered with their movement in host embryos with normal adhesion. To exclude the possibility that the observed effects in movement directionality are mere secondary consequences of cell sorting due to differential adhesion between donor and host cells, we analyzed mesendoderm movement behavior in *e-cadherin* mutant and morphant embryos with uniformly reduced adhesion at midgastrulation stages (7–9 hpf). We found that in both *e-cadherin* mutant and morphant embryos, movement directionality of mesendoderm progenitors was clearly reduced, as determined by their instantaneous speed, displacement speed, and displacement effectiveness in two-photon excitation microscopy movies detecting nuclei (Figures 5A–5C). This indicates that uniform reduction of cell-cell adhesion has consequences for individual mesendoderm cell movements similar to those observed for transplanted cells with reduced adhesion. We also found that movement coordination among mesendoderm progenitors decreased with increasing distance between cells and was strongly reduced in both *e-cadherin* mutant and morphant embryos, as determined by their movement similarity (Figures 5D–5F; Figure S1), suggesting that movement coordination depends on cell-cell adhesion.

Our suggestion that E-cadherin-mediated mechanical coupling of cells is critical for directed movement of mesendoderm progenitors is based on the observation that E-cadherin-dependent cell-cell adhesion strength and effective movement speed are strongly correlated with each other. However, this does not exclude the possibility that E-cadherin-mediated processes other than adhesion, such as mesendoderm cell differentiation and proliferation, might also be involved. We therefore investigated potential adhesion-independent functions of E-cadherin in mesendoderm cells by analyzing downstream signaling through β-catenin [11], cell differentiation, and cell proliferation [12], but were unable to detect any significant changes between wild-type and E-cadherin defective mesendoderm cells (Figure S2; [13–16]). These findings support our suggestion that E-cadherin functions in mesendoderm movement directionality by modulating cell adhesion rather than adhesion-independent processes.

To determine how E-cadherin-mediated adhesion of mesendoderm progenitors controls movement directionality and coordination, we recorded high-magnification differential interference contrast (DIC) movies of lateral mesendoderm progenitors in wild-type and *e-cadherin* morphant embryos during midgastrulation stages (7–9 hpf). Analysis of cell morphology and movement showed that migrating wild-type mesendoderm progenitors formed stable cell-cell contacts and, once the contact had formed, moved only very little relative to each other (Figures 5G–5J; Movie S2). In contrast, *e-cadherin* morphant mesendoderm progenitors failed to form stable cell-cell contacts and restrict their movements relative to each other (Figures 5G–5J; Movie S3), resulting in progenitors frequently crawling over each other, a behavior only rarely observed in wild-type embryos. These observations suggest that E-cadherin-mediated adhesion of mesendoderm progenitors enhances cell-cell contact persistency and, at the same time, restricts movement of cells relative to each other.

Cell-cell adhesion might function specifically in collective migration or, alternatively, might have additional functions in single-cell migration, e.g., regulating mesendoderm cell adhesion to the overlying ectoderm and/or underlying yolk syncytial layer. To distinguish between these possibilities, we transplanted a small number of differentially labeled control and *e-cadherin* MO cells into MZ*oep* mutants and analyzed their migratory behavior. We found that the migration directionality of transplanted single mesendoderm progenitors remained unchanged when E-cadherin expression was reduced (Figure S3), indicating that cell-cell adhesion is specifically required during collective migration but is largely dispensable for single-cell migration in this system. It also suggests that E-cadherin is not needed for cell migration per se but is specifically required to undergo directed movement during collective migration.

Taken together, these findings show that individual mesendoderm progenitors must adhere to each other to participate

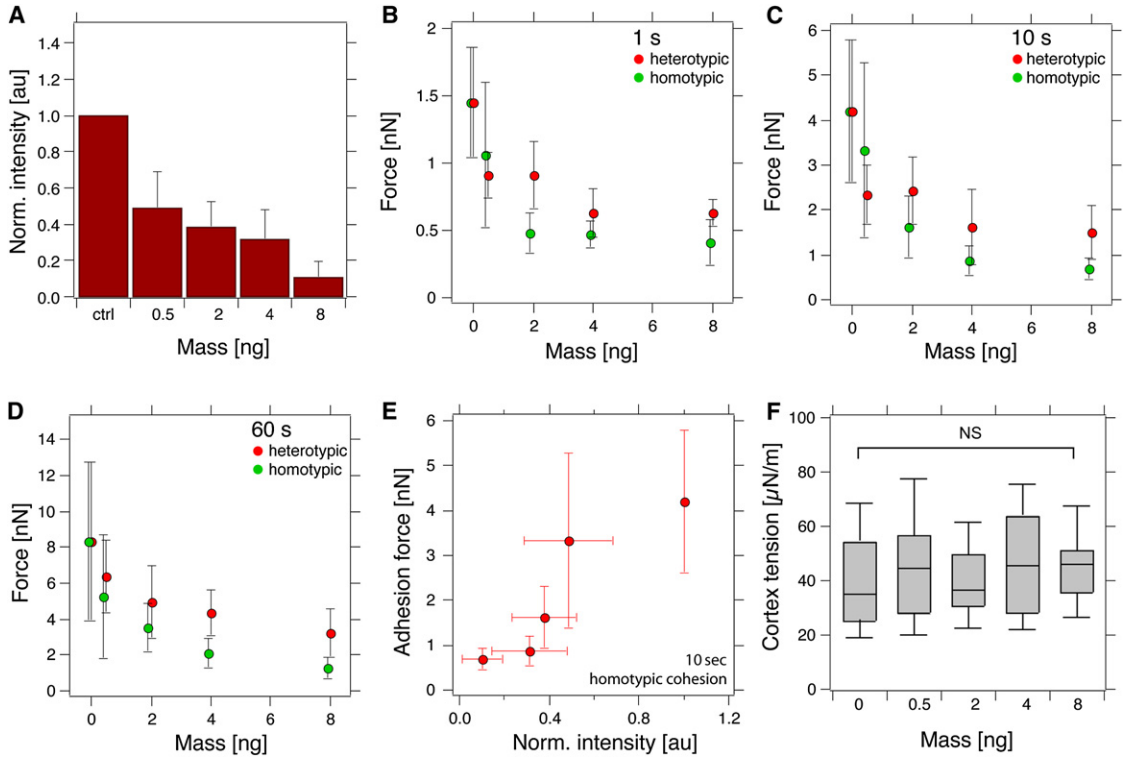

Figure 3. Regulation of Mesendoderm Cell-Cell Adhesion

(A) E-cadherin at the plasma membrane of mesendoderm progenitors injected with increasing amounts of *e-cadherin morpholino* (MO) as determined by in vitro biotinylation. Staining intensity of biotinylated E-cadherin in *e-cadherin* morphant cells is shown relative to mesendoderm WT control cells (ctrl; mean ± standard deviation).

(B–D) Homotypic (green) and heterotypic (red) adhesion force of mesendoderm progenitors injected with increasing amounts of *e-cadherin* MO for 1 s (B), 10 s (C), and 60 s (D) contact time, measured by single-cell force spectroscopy [10].

(E) Homotypic adhesion force as a function of the normalized E-cadherin staining intensity as shown in (A) of WT control and *e-cadherin* MO injected progenitor cells (median ± median average deviation [MAD]).

(F) Cortex tension of mesendoderm progenitors injected with increasing amounts of *e-cadherin* MO.

in directed movement during collective migration. It further indicates that the ability of single mesendoderm progenitors to undergo directed migration is not sufficient to achieve directed movement when part of a group.

Generally, collective migration has a cell-autonomous movement component, defined by the migratory activity of individual cells, and a nonautonomous (or advective) component, describing the translocation of individual cells by the global movement of the cluster [1, 2]. Our finding that individual mesendoderm progenitors in the absence of neighboring cells migrate normally indicates that directed migration is an individual cell property rather than being set de novo by a particular collective/group property. However, once mesendoderm progenitors move as part of a group, cell-cell adhesion mediation of movement becomes critical to their directed movement. Why do cells need cell-cell adhesion to maintain their directionality when moving together? Individual cells, although globally moving in the same direction during collective migration, exhibit some degree of variability in their individual movement paths (Figure 1). It is possible that this variability is reduced when cells are coupled together through cell-cell adhesion, resulting in more directed movements of adherent cells compared to nonadherent cells. To determine the plausibility of this assumption, we have analyzed the contribution of cell-cell adhesion to collective mesendoderm migration using a numerical simulation. In our simulation, the migration of mesendoderm progenitors is mediated by four different force types: (1) a short-range spring force (f_s) modeling cell-cell adhesion, (2) a chemotactic force (f_c) modeling polarized cell migration, (3) a "Vicsek" force (f_v) modeling collective migration [17], and (4) a noise force (f_n) modeling random cell migration (for details, see Supplemental Experimental Procedures). The "Vicsek" force is based on a model illustrating that for a system of self-driven particles (cells), local interactions can give rise to a kinetic phase transition between a globally disordered state (zero average cell velocity) and a state with large-scale order and nonzero average cell velocity (collective migration). We have included the "Vicsek" force in our simulation because it has previously been shown to accurately describe a variety of collective biological phenomena, ranging from the rotation of bacterial colonies [18] to the collective migration of epidermal keratocyte cells [19]. Using the relative differences in cell-cell adhesion strength between wild-type control and *e-cadherin* morphant cells (Figure 3) to determine the spring force (f_s) in our simulation, we found that morphant cells exhibit less directed and slower movement compared to wild-type control cells during collective migration (Figure S4). These findings are consistent with our experimental observations and thus confirm the plausibility of our proposed mechanism.

Although this simulation illustrates that transplanted cells with reduced cell-cell adhesion move in a less-directed

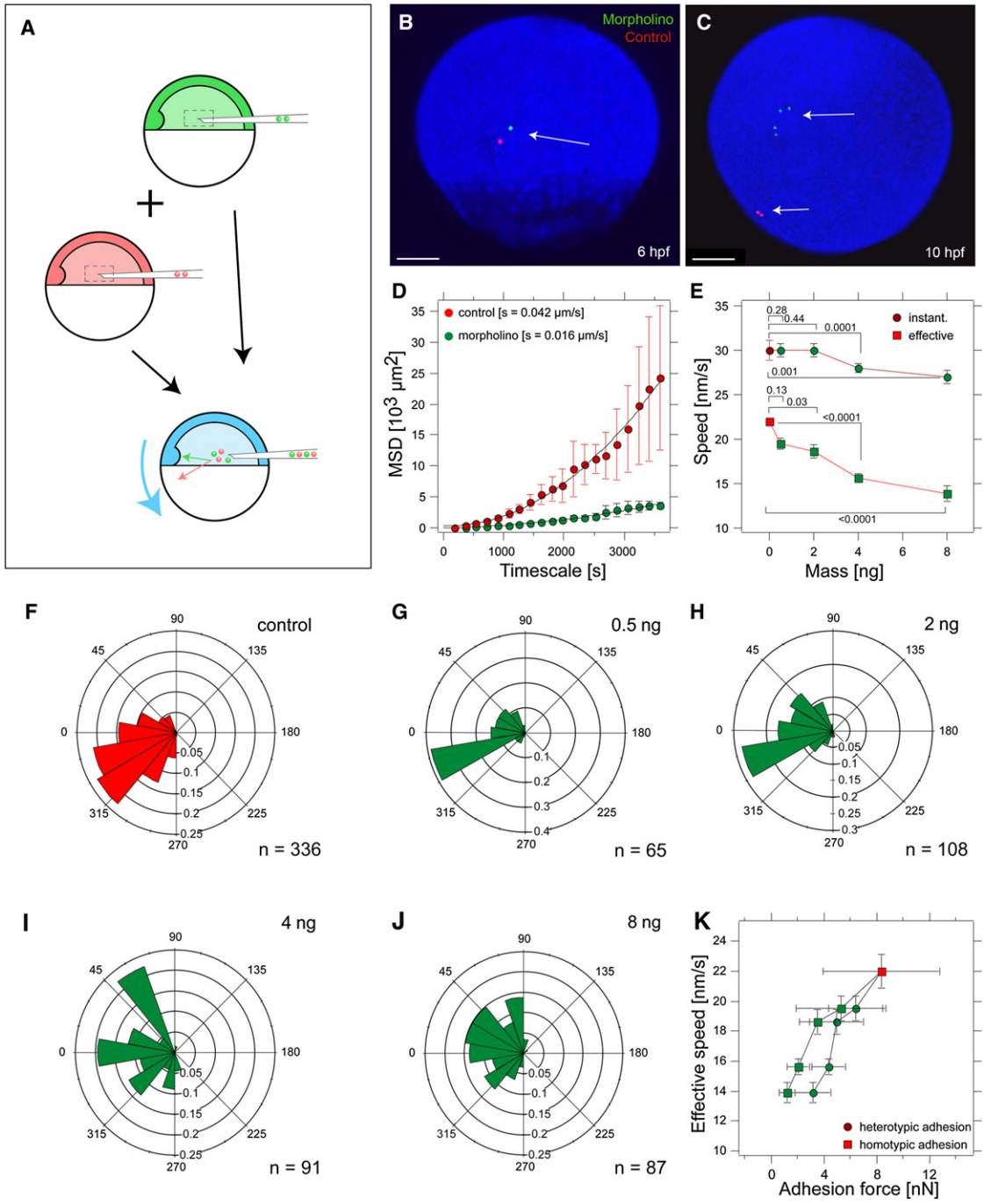

Figure 4. Effect of Cell-Cell Adhesion on Individual Mesendoderm Cell Movement

(A) Schematic representation of the transplantation experiment. Cells from donor embryos (red, control; green, *e-cadherin* morphant) are transplanted into a host WT embryo (blue) at 50% epiboly (5 hpf). The movement of the cells until the end of gastrulation (10 hpf) was monitored by time-lapse confocal microscopy.

(B and C) Transplanted *e-cadherin* morphant (green) and WT control (red) cells at the onset of gastrulation (6 hpf; B) and at the end of gastrulation (10 hpf; C). Arrows point to transplanted cells.

(D) MSD plot of *e-cadherin* morphant and WT control cells.

(E) Average instantaneous (circles) and average effective (squares) movement speed for WT control (red) and *e-cadherin* morphant (green) cells. Error bars represent standard error of the mean. p values determined by t test are shown above or below the brackets.

(F–J) Movement orientation of WT control (red; F) and *e-cadherin* morphant (green) cells injected with 0.5 ng (G), 2 ng (H), 4 ng (I), and 8 ng (J) *e-cadherin morpholino* (MO) per embryo represented as angular histograms. Angles were calculated with respect to the dorsal-pointing vector originating from the embryo center. n represents number of analyzed cells.

(K) Average effective movement speed (mean ± standard error of the mean) as a function of the heterotypic and homotypic adhesion force (median ± MAD) of WT control (red) and *e-cadherin* morphant (green) cells as measured in Figure 2D (60 s contact time). n represents number of analyzed cells.

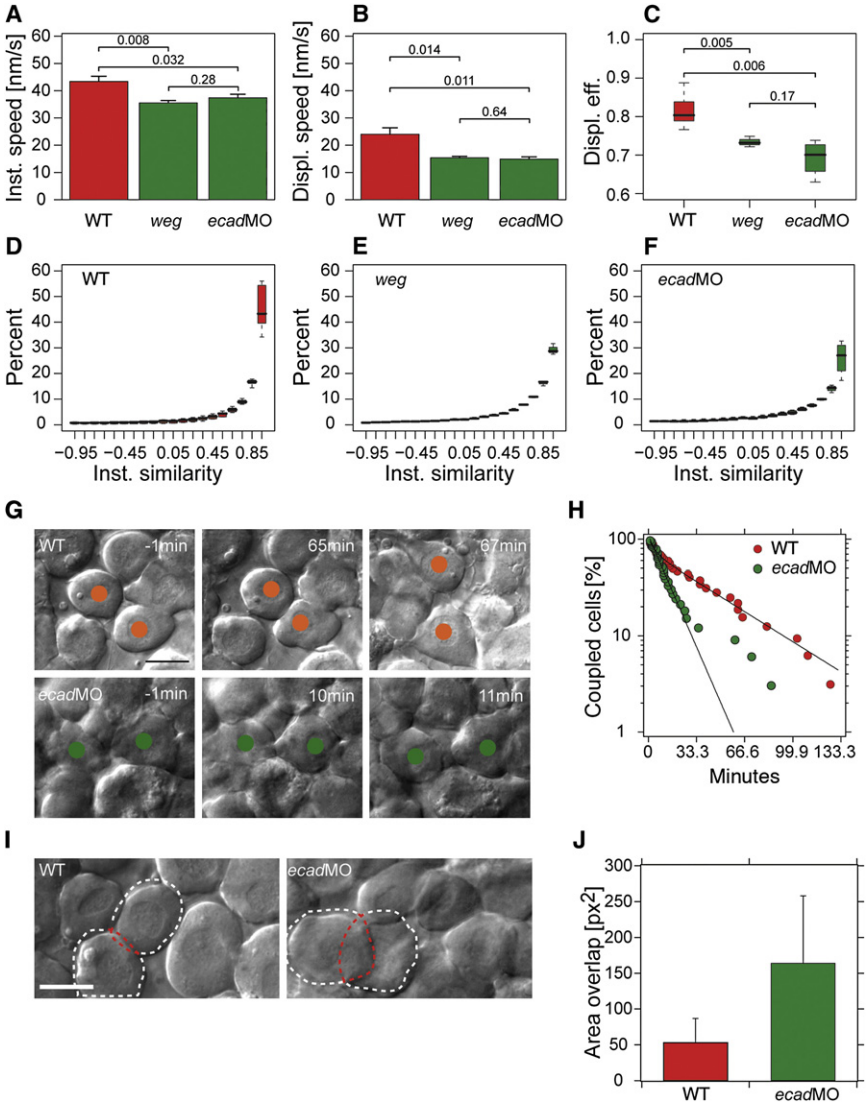

Figure 5. Movement of Lateral Mesendoderm Cells in *e-cadherin* Mutant and Morphant Embryos

(A–C) Average instantaneous speed (A), average displacement speed (B), and displacement effectiveness (C) of mesendoderm progenitor cell movements during midgastrulation stages (7–9 hpf). Data of 6 wild-type (WT; red), 3 *e-cadherin/weg* mutant (*weg*; green), and 4 *e-cadherin* morphant (*ecad*MO; green; 4 ng per embryo) embryos are shown. Error bars in (A) and (B) represent the standard error of the mean, and in (C) the standard deviation. p values determined by t test are shown above the brackets. The average number of tracked cells per embryo is 390 ± 169 in WT, 403 ± 213 in mutant, and 380 ± 121 in morphant embryos.

(D–F) Instantaneous similarity of neighboring mesendoderm progenitor movements within a maximum distance of 20 μm in WT (D), *e-cadherin/weg* mutant (E), and *e-cadherin* morphant (F) embryos. Values range from −1.0 (opposite direction of movement) over 0 (movement vectors are orthogonal) to +1 (parallel movement). Histograms were generated separately for each embryo. Box plots show the distribution of the bin heights among the different embryos.

(G) Series of consecutive images from differential interference contrast (DIC) movies showing exemplary mesendoderm progenitor cell couplets in WT (red) and *e-cadherin* morphant embryos (green; 4 ng MO per embryo) from cell-cell contact formation (−1 min) to contact separation (67 min for WT and 11 min for morphant cells) during their migration at midgastrulation stages (7–9 hpf). Scale bar represents 16 μm.

(H) Cumulated histogram of cell contact times of two mesendoderm cells in WT and *e-cadherin* morphant embryos (4 ng per embryo). Number of interacting cells decreases exponentially with higher contact time. Solid line represents a single-exponential decay with a mean contact survival time t = 12.5 ± 0.3 min and t = 28 ± 1.7 min for morphant (*ecad*MO) and WT cells, respectively.

(I) DIC image outlining the overlap area of representative mesendoderm couplets in WT and *e-cadherin* morphant embryos (4 ng per embryo). Cell couplets are outlined with a white line and the overlap with a red line. Scale bar represents 18 μm.

(J) Overlap area (outlined in I) between two mesendoderm cells in WT and *e-cadherin* morphant embryos.

manner than their neighboring cells with normal adhesion (Figure 4), it does not explain why a cell moving alone exhibits similar movement directionality to cells moving as a coherent cluster (Figure 2). The most likely explanation for this is that a cell, when moving as part of a group, displays a higher degree of movement variability than a cell moving alone and therefore needs to adhere to neighboring cells in order to reduce this variability. Why should a cell have increased movement variability when moving as part of a group? One likely possibility is that positional cues guiding the migration of mesendoderm progenitors are less interpretable for a cell when moving as part of a group rather than alone. This could be caused by the binding and/or internalization of guidance cues by the migrating cells themselves, which reduces the availability and distribution of these cues within the group. Indeed, endocytosis of signaling molecules such as DPP and FGF8 has recently been shown to alter their graded distribution within both vertebrate and invertebrate tissues [20, 21]. Further studies identifying the molecules guiding mesendoderm progenitor migration and their distribution within the mesendoderm will be needed to elucidate the molecular mechanisms underlying collective versus individual progenitor cell movements.

Adhesion-mediated cell-cell contact formation has previously been shown to be critical for movement coordination during collective migration of culture cells [22] and various cell types in development, including *Drosophila* border cells [23, 24], the zebrafish lateral line primordium [25, 26], and mesoderm progenitors during vertebrate gastrulation [27–32]. Additionally, contact inhibition has recently been shown to direct the coherent migration zebrafish neural crest cells [33], suggesting a function for cell-cell contacts in determining the direction of coherent migration. A common feature of cell-cell contact inhibition and adhesion is that protrusive

activity and consequently locomotion is inhibited at the site of contact. This contact-induced inhibition of movement can both polarize individual cell movements and, at the same time, reduce movement variability among comigrating cells. Interestingly, although contact inhibition between neural crest cells has been suggested to establish their movement directionality de novo [33], we show that cell-cell adhesion between mesendoderm progenitors is primarily required for the directed migration of individual cells undergoing collective migration. Future studies will have to unravel common and divergent features of cell adhesion and cell contact inhibition in modulating individual cell movements during collective migration.

Experimental Procedures

Embryo Staging and Maintenance

Fish maintenance and embryo collection were carried out as described [34]. Embryos were grown at 31°C in E3 medium and staged according to [35].

mRNA and Morpholino Oligonucleotide Injections

mRNA was synthesized as described [15]. To generate mesendoderm progenitors, we injected one-cell-stage wild-type Tup Longfin (TL) embryos with either a mix of *cyclops* (*cyc*) mRNA (100 pg) and *H2A-zf::mcherry* mRNA (100 pg) for control cells or a mix of *cyclops* (*cyc*) mRNA (100 pg), *e-cadherin* MO, and Alexa Fluor 488 conjugated histone H1 (1 mg/ml, H13188, Invitrogen) for experimental cells. To reduce E-cadherin expression, we injected discrete concentrations (0.5–8 ng per embryo) of a previously described *e-cadherin* MO [14] (5′-ATCCCACAGTTGTTACACAAGCCAT-3′) into one-cell-stage embryos.

Transplantation Experiments

Wild-type TL and MZ*oep* mutant donor and host embryos were dechorionated with Pronase (2 mg/ml in E2) and transferred into an agarose plate with E3 medium. One to two cells were taken from control and experimental donor embryos at 50% epiboly stage (5 hpf) and transplanted into the emerging lateral mesendoderm of a host embryo labeled with Dextran Alexa Fluor 647 at shield stage (6 hpf).

E-Cadherin and β-Catenin Whole-Mount Antibody Staining

Wild-type embryos and *e-cadherin* morphant embryos (4 ng MO per embryo) were incubated at 31°C and fixed at 7.5 hpf in 4% paraformaldehyde at 4°C overnight. Samples were blocked with serum and incubated overnight with β-catenin (1:600, Sigma) and E-cadherin primary (1:200) antibodies. The primary antibodies were visualized by using Alexa Fluor 488 goat anti-mouse (1:500, Molecular Probes) for β-catenin and Cy5-conjugated goat anti-rabbit IgG (1:500, Jackson Laboratories) for E-cadherin detection. Images were obtained with an upright Leica SP5 confocal microscope equipped with a 20× water immersion lens with 488 Argon and 633 HeNe laser lines.

Cell Surface Biotinylation and E-Cadherin Detection

Cell surface biotinylation and E-cadherin detection experiments were carried out as described [10]. Whole protein content was estimated via Coomassie-stained SDS polyacrylamide gel electrophoresis of extracellular protein fraction. As a loading control, a silver stain of SDS gels was conducted.

Differential Interference Contrast Microscopy

Images were obtained with a Zeiss Axioplan 2 microscope equipped with a 40× water immersion lens and a QImaging Retiga-SRV Fast 1394 camera. Frames were captured at 63 s intervals for 2 hr (6–8 hpf). The temperature was kept constant during image acquisition (24°C). For cell tracking and measurements of cell-cell overlap area and contact time, Fiji software was used and statistic analysis was done with IGOR Pro software. Wild-type and *e-cadherin* morphant embryos (4 ng MO per embryo) were incubated at 31°C, dechorionated at 6 hpf with Pronase (2 mg/ml), and mounted in 1% agarose for subsequent imaging.

Confocal Microscopy

Movies of embryos containing transplanted cells were obtained with an upright Leica SP5 confocal microscope equipped with a 10× and 20× water immersion lens with 488 Argon, DPSS 561, and 633 HeNe laser lines. Images were taken in lateral regions of the gastrula at 3 min time intervals during mid to late gastrulation stages (7–10 hpf). The temperature was kept constant in all movies (28°C).

Two-Photon Excitation Microscopy

Two-photon excitation imaging of nuclear movements was performed as described [36]. Images were taken in lateral regions of wild-type, *e-cadherin* morphant, and *e-cadherin/weg* mutant embryos at 1 min time intervals during midgastrulation stages (7–9 hpf). The temperature was kept constant in all movies (28°C).

Statistical Data Processing

Force spectroscopy data are represented as median ± median average deviation and were computed with IGOR Pro if not differently indicated. Migration data were normally distributed and are presented as mean ± standard error of the mean (Figure S5). Pearson's product-moment correlation coefficients and their statistical significance were computed with R. Histograms were compiled in IGOR Pro, and bin width was set according to Rice's rule (width = $2(n)^{1/3}$), with n representing number of observations.

Image Analysis

Tracking and analysis of cell and nuclei movements in wild-type, *e-cadherin* morphant, and *e-cadherin/weg* mutant embryos were done with custom-built nuclei tracking software [8]. The figures for instantaneous similarity, instantaneous speed, displacement speed, and displacement effectiveness were plotted with R. For tracking transplanted cells in three dimensions (x, y, and z), IMARIS 6.2.0 software was used. The statistical analysis was done with IGOR Pro software. Tracks of transplanted cells were analyzed in 3D via home-built IGOR Pro procedures to extract mean squared displacement (MSD) $< \Delta x^2 >$ with N representing number of frames and n representing number of time intervals:

$$\langle \Delta x^2 \rangle = \frac{1}{N-n+1} \sum_{i=0}^{N-n} (x_{n+i} - x_i)^2 + (z_{n+i} - z_i)^2 + (y_{n+i} - y)^2$$

Circumferential movement of a particle on a sphere would yield lower displacements for longer time intervals. Therefore, individual cell tracks were corrected for the intrinsic curvature of the embryo according to

$$\langle \Delta x^2_{corr} \rangle = \left[2R_E \cdot \arcsin\left(\frac{\sqrt{\langle \Delta x^2 \rangle}}{2R_E} \right) \right]^2,$$

with R_E representing the embryo radius and $\langle \Delta x^2_{corr} \rangle$ representing the corrected and $\langle \Delta x^2 \rangle$ the uncorrected mean squared displacement. MSD plots were fitted to a second-order polynomial $\langle \Delta x^2_{corr} \rangle (t) = s^2 t^2 + Dt$ to extract effective migration speed s and diffusion coefficient D [37]. Instantaneous speed v_i was calculated with the distance Δd a cell traveled within two subsequent frames separated by a frame rate f = 1/t: $v_i = \frac{\Delta d}{\Delta t}$.

Movement orientation was calculated from projected stacks. The angle between the displacement vector of the cells in the last frame in respect to the dorsal-pointing Einheitsvector was calculated as

$$\cos\alpha = \frac{\vec{x} \cdot \vec{y}}{|\vec{x}| \cdot |\vec{y}|}.$$

The instantaneous similarity of movement between cells i and j is defined as the scalar product of their instantaneous speed vectors:

$$S_{ij}(t) = \frac{\langle \vec{v}_i(t), \vec{v}_j(t) \rangle}{|\vec{v}_i(t)||\vec{v}_j(t)|} = \cos\theta.$$

Displacement speed was calculated by measuring the overall movement distance between the initial position at t_0 and the final position at t_m of each cell's trajectory divided by the movement time:

$$D = \frac{|\vec{x}(t_m) - \vec{x}(t_0)|}{t_m - t_0}.$$

The displacement effectiveness of a cell was measured by taking the overall movement distance normalized to the length of the trajectory. The length of a trajectory can be estimated as the sum of the instantaneous velocity vectors:

$$E = \frac{|\vec{x}(t_m) - \vec{x}(t_0)|}{L}, L = \sum_{s=0}^{m} \vec{v}(t_s).$$

Because shorter cell trajectories would usually show a better displacement effectiveness than long cell trajectories, only those trajectories were quantified where the cell could be tracked for at least 20 time points.

Cell-cell overlap area in the DIC movies was determined by measuring the thickness of the overlap with ImageJ. The overlap area A_O was calculated by approximating the cells by a sphere. Half the thickness of the overlapping zone corresponds to the height of a circle segment h in one cell. The area of each of the segments can then be calculated by

$$A_O = 2 \cdot \frac{R_c^2}{2} \cdot (\alpha - \sin\alpha)$$
$$\alpha = \arccos\left(\frac{R_c - h}{R_c}\right),$$

where R_C is the averaged diameter of the two interacting cells and α is the arc angle.

Atomic Force Microscopy-Based Single-Cell Force Spectroscopy

Single-cell force spectroscopy (SCFS) was essentially carried out as described [10]. Briefly, atomic force microscopy (AFM) cantilevers (MLCT, Veeco) were plasma cleaned and incubated in 2.5 mg/ml ConA at 4°C overnight. Cantilevers were calibrated via the thermal noise method before each adhesion measurement. Cells were attached to the cantilevers with ConA via a contact force of 1 nanonewton (nN). Approach and retraction velocity was set to 10 μm/s, and contact time was varied between 1 s and 1 min. Cell-cell contact force was set to 1 nN.

Cortex Tension Measurement

Cortex tension measurements were acquired as described [10]. Briefly, control and experimental mesendoderm cells were seeded into a homemade reaction container and indented with a colloidal force probe (d = 5 μm). Approach and retract velocity was set to 1 μm/s, and contact force was reduced to 500 piconewtons (pN). To extract cortex tension, we fitted the contact force of the approach curve between 125 and 250 pN to the liquid droplet model [10].

Supplemental Information

Supplemental Information includes Supplemental Experimental Procedures, five figures, and three movies and can be found with this article online at doi:10.1016/j.cub.2009.11.036.

Acknowledgments

We are grateful to A. Oates, E. Paluch, E. Raz, L. Rohde, P. Tomancak, and members of the Heisenberg laboratory for reading earlier versions of this manuscript; I. Richter for help with western blotting; and J. Helenius for help with programming. We thank L. Carvalho for providing imaging data, P. Stockinger for providing the N-cadherin antibody, M. Braer for help with cell tracking, S. Grill for valuable discussions and participation in the fifth floor seminar club, the microscopy facility of the Max Planck Institute of Molecular Cell Biology and Genetics and the Biotechnology Center at Technische Universität Dresden for continuous support, and the fish facility for excellent fish care. This work was supported by grants from Boehringer Ingelheim Fonds to M.K., the Max Planck Society, the German Research Foundation, and the European Community (ZF-Models, ZF-Cancer, Endotrack) to C.-P.H.

Received: July 16, 2009
Revised: October 19, 2009
Accepted: November 11, 2009
Published online: January 14, 2010

References

1. Montell, D.J. (2008). Morphogenetic cell movements: Diversity from modular mechanical properties. Science *322*, 1502–1505.
2. Friedl, P., and Gilmour, D. (2009). Collective cell migration in morphogenesis, regeneration and cancer. Nat. Rev. Mol. Cell Biol. *10*, 445–457.
3. Insall, R.H., and Jones, G.E. (2006). Moving matters: Signals and mechanisms in directed cell migration. Nat. Cell Biol. *8*, 776–779.
4. Deisboeck, T.S., and Couzin, I.D. (2009). Collective behavior in cancer cell populations. Bioessays *31*, 190–197.
5. Buhl, J., Sumpter, D.J., Couzin, I.D., Hale, J.J., Despland, E., Miller, E.R., and Simpson, S.J. (2006). From disorder to order in marching locusts. Science *312*, 1402–1406.
6. Haas, P., and Gilmour, D. (2006). Chemokine signaling mediates self-organizing tissue migration in the zebrafish lateral line. Dev. Cell *10*, 673–680.
7. Sepich, D.S., Calmelet, C., Kiskowski, M., and Solnica-Krezel, L. (2005). Initiation of convergence and extension movements of lateral mesoderm during zebrafish gastrulation. Dev. Dyn. *234*, 279–292.
8. Carvalho, L., Stühmer, J., Bois, J.S., Kalaidzidis, Y., Lecaudey, V., and Heisenberg, C.P. (2009). Control of convergent yolk syncytial layer nuclear movement in zebrafish. Development *136*, 1305–1315.
9. Gritsman, K., Zhang, J., Cheng, S., Heckscher, E., Talbot, W.S., and Schier, A.F. (1999). The EGF-CFC protein one-eyed pinhead is essential for nodal signaling. Cell *97*, 121–132.
10. Krieg, M., Arboleda-Estudillo, Y., Puech, P.H., Käfer, J., Graner, F., Müller, D.J., and Heisenberg, C.P. (2008). Tensile forces govern germ-layer organization in zebrafish. Nat. Cell Biol. *10*, 429–436.
11. Nelson, W.J., and Nusse, R. (2004). Convergence of Wnt, beta-catenin, and cadherin pathways. Science *303*, 1483–1487.
12. Gumbiner, B.M. (1996). Cell adhesion: The molecular basis of tissue architecture and morphogenesis. Cell *84*, 345–357.
13. Shimizu, T., Yabe, T., Muraoka, O., Yonemura, S., Aramaki, S., Hatta, K., Bae, Y.K., Nojima, H., and Hibi, M. (2005). E-cadherin is required for gastrulation cell movements in zebrafish. Mech. Dev. *122*, 747–763.
14. Babb, S.G., and Marrs, J.A. (2004). E-cadherin regulates cell movements and tissue formation in early zebrafish embryos. Dev. Dyn. *230*, 263–277.
15. Montero, J.A., Carvalho, L., Wilsch-Bräuninger, M., Kilian, B., Mustafa, C., and Heisenberg, C.P. (2005). Shield formation at the onset of zebrafish gastrulation. Development *132*, 1187–1198.
16. Kane, D.A., McFarland, K.N., and Warga, R.M. (2005). Mutations in half baked/E-cadherin block cell behaviors that are necessary for teleost epiboly. Development *132*, 1105–1116.
17. Vicsek, T., Czirók, A., Ben-Jacob, E., Cohen, I.I., I, and Shochet, O. (1995). Novel type of phase transition in a system of self-driven particles. Phys. Rev. Lett. *75*, 1226–1229.
18. Czirók, A., Ben-Jacob, E., Cohen, I.I., I, and Vicsek, T. (1996). Formation of complex bacterial colonies via self-generated vortices. Phys. Rev. E Stat. Phys. Plasmas Fluids Relat. Interdiscip. Topics *54*, 1791–1801.
19. Szabó, B., Szöllösi, G.J., Gönci, B., Jurányi, Z., Selmeczi, D., and Vicsek, T. (2006). Phase transition in the collective migration of tissue cells: Experiment and model. Phys. Rev. E Stat. Nonlin. Soft Matter Phys. *74*, 061908.
20. Entchev, E.V., Schwabedissen, A., and González-Gaitán, M. (2000). Gradient formation of the TGF-beta homolog Dpp. Cell *103*, 981–991.
21. Yu, S.R., Burkhardt, M., Nowak, M., Ries, J., Petrásek, Z., Scholpp, S., Schwille, P., and Brand, M. (2009). Fgf8 morphogen gradient forms by a source-sink mechanism with freely diffusing molecules. Nature *461*, 533–536.
22. Vitorino, P., and Meyer, T. (2008). Modular control of endothelial sheet migration. Genes Dev. *22*, 3268–3281.
23. Melani, M., Simpson, K.J., Brugge, J.S., and Montell, D. (2008). Regulation of cell adhesion and collective cell migration by hindsight and its human homolog RREB1. Curr. Biol. *18*, 532–537.
24. Niewiadomska, P., Godt, D., and Tepass, U. (1999). DE-Cadherin is required for intercellular motility during Drosophila oogenesis. J. Cell Biol. *144*, 533–547.
25. Kerstetter, A.E., Azodi, E., Marrs, J.A., and Liu, Q. (2004). Cadherin-2 function in the cranial ganglia and lateral line system of developing zebrafish. Dev. Dyn. *230*, 137–143.
26. Wilson, A.L., Shen, Y.C., Babb-Clendenon, S.G., Rostedt, J., Liu, B., Barald, K.F., Marrs, J.A., and Liu, Q. (2007). Cadherin-4 plays a role in the development of zebrafish cranial ganglia and lateral line system. Dev. Dyn. *236*, 893–902.
27. Chen, X., and Gumbiner, B.M. (2006). Paraxial protocadherin mediates cell sorting and tissue morphogenesis by regulating C-cadherin adhesion activity. J. Cell Biol. *174*, 301–313.
28. Yang, X., Chrisman, H., and Weijer, C.J. (2008). PDGF signalling controls the migration of mesoderm cells during chick gastrulation by regulating N-cadherin expression. Development *135*, 3521–3530.
29. Warga, R.M., and Kane, D.A. (2007). A role for N-cadherin in mesodermal morphogenesis during gastrulation. Dev. Biol. *310*, 211–225.
30. Radice, G.L., Rayburn, H., Matsunami, H., Knudsen, K.A., Takeichi, M., and Hynes, R.O. (1997). Developmental defects in mouse embryos lacking N-cadherin. Dev. Biol. *181*, 64–78.

31. Horikawa, K., Radice, G., Takeichi, M., and Chisaka, O. (1999). Adhesive subdivisions intrinsic to the epithelial somites. Dev. Biol. *215*, 182–189.
32. Winklbauer, R., Selchow, A., Nagel, M., and Angres, B. (1992). Cell interaction and its role in mesoderm cell migration during Xenopus gastrulation. Dev. Dyn. *195*, 290–302.
33. Carmona-Fontaine, C., Matthews, H.K., Kuriyama, S., Moreno, M., Dunn, G.A., Parsons, M., Stern, C.D., and Mayor, R. (2008). Contact inhibition of locomotion in vivo controls neural crest directional migration. Nature *456*, 957–961.
34. Westerfield, M. (2000). The Zebrafish Book, Fourth Edition (Eugene, OR: University of Oregon Press).
35. Kimmel, C.B., Ballard, W.W., Kimmel, S.R., Ullmann, B., and Schilling, T.F. (1995). Stages of embryonic development of the zebrafish. Dev. Dyn. *203*, 253–310.
36. Ulrich, F., Concha, M.L., Heid, P.J., Voss, E., Witzel, S., Roehl, H., Tada, M., Wilson, S.W., Adams, R.J., Soll, D.R., and Heisenberg, C.P. (2003). Slb/Wnt11 controls hypoblast cell migration and morphogenesis at the onset of zebrafish gastrulation. Development *130*, 5375–5384.
37. Qian, H., Sheetz, M.P., and Elson, E.L. (1991). Single particle tracking. Analysis of diffusion and flow in two-dimensional systems. Biophys. J. *60*, 910–921.